PROCEEDINGS OF SPIE

SPIEDigitalLibrary.org/conference-proceedings-of-spie

# Sub-ps 1030 nm laser-induced damage threshold evaluation of pulsed-laser deposited sesquioxides and magnetron-sputtered metal oxide optical coatings

Marek Stehlík, Goby Govindassamy, Janis Zideluns, Fabien Lemarchand, Frank Wagner, et al.

Marek Stehlík, Goby Govindassamy, Janis Zideluns, Fabien Lemarchand, Frank Wagner, Julien Lumeau, Jacob Mackenzie, Laurent Gallais, "Sub-ps 1030 nm laser-induced damage threshold evaluation of pulsed-laser deposited sesquioxides and magnetron-sputtered metal oxide optical coatings," Proc. SPIE 12300, Laser-Induced Damage in Optical Materials 2022, 123000G (2 December 2022); doi: 10.1117/12.2641792

SPIE.

Event: SPIE Laser Damage, 2022, Rochester, New York, United States

# Sub-ps 1030 nm laser-induced damage threshold evaluation of pulsed-laser deposited sesquioxides and magnetron-sputtered metal oxide optical coatings

Marek Stehlík[a], Goby Govindassamy[b], Janis Zideluns[a], Fabien Lemarchand[a], Frank Wagner[a], Julien Lumeau[a], Jacob Mackenzie[b], and Laurent Gallais[a]

[a]Aix Marseille Univ, CNRS, Centrale Marseille, Institut Fresnel, Marseille, France
[b]Zepler Institute - Optoelectronics Research Centre, University of Southampton, Highfield, Southampton SO17 1BJ, UK

## ABSTRACT

Crystalline sesquioxide films ($Sc_2O_3$, $Y_2O_3$, $Lu_2O_3$) produced by pulsed-laser deposition were examined for laser damage resistance with pulses of 500 fs duration, at a wavelength of 1030 nm and at a 10 Hz repetition rate. Comparable tests were performed with amorphous magnetron-sputtered thin films ($SiO_2$, $HfO_2$, $Nb_2O_5$). We found the laser-induced damage thresholds of the sesquioxides are close to those of $HfO_2$ in the multi-pulse test regime. The results are the basis for designs of damage resistant reflective components used in ultrashort-pulse lasers.

**Keywords:** Pulsed-laser deposition, Laser-induced damage testing, Sesquioxides, Metal oxides, Sub-picosecond regime

## 1. INTRODUCTION

The laser-induced damage threshold (LIDT) of optical components based on coatings is the limiting factor for ultrashort pulse high-power laser operation. To enhance the LIDT of optical coatings, testing of extensive spectrum of materials,[1–3] development of novel optimal coating designs,[4–6] and comparison between deposition methods have all been done.[7–9] Among the available thin-film growth methods, pulsed-laser deposition (PLD) is one of the most versatile and powerful.[10] PLD has been used to deposit a broad range of materials,[11] and has recently proven to be a viable method for optical coating fabrication.[12–16]

In the last decade, mirrors made of $HfO_2$, a high-refractive-index material, and $SiO_2$, a low-refractive-index material, received substantial attention.[4,17,18] However, LIDT studies for $Sc_2O_3$ or $Y_2O_3$ films reported in the sub-picosecond (ps) range suggest that sesquioxides might be a suitable alternative for $HfO_2$.[9,19–21] In particular, $Sc_2O_3$ is a potential high-index material with a slightly higher optical bandgap (5.7 eV)[22] than $HfO_2$ (5.55 eV).[23,24] To our knowledge, all LIDT studies on sesquioxides have been performed on either amorphous or polycrystalline films. Consequently, the LIDT results might differ from films made using the PLD method, which has the potential to grow single-crystal films.[15,25,26]

In this study, we produced pulsed-laser deposited crystalline sesquioxide films ($Sc_2O_3$, $Y_2O_3$, $Lu_2O_3$) and evaluated them for laser damage with pulses of 500 fs duration, at a wavelength of 1030 nm and at a 10 Hz repetition rate. The LIDT tests were carried out also with amorphous magnetron-sputtered thin films of well-known optical-coating materials ($SiO_2$, $HfO_2$, $Nb_2O_5$), whose results served as a benchmark. The LIDT values for these more common materials have already been reported in studies comparing them to a variety of optical-coating materials.[1,24]

The thin films investigated here are intended for application in dielectric multilayer mirrors or diffractive gratings, namely grating waveguide structures (GWSs).[27] The later optical components allow control of the temporal,[28] spectral[29] and spatial profiles of light within or from high-power laser systems.[30] In this work, sesquioxides in their crystalline form and amorphous metal oxides are being investigated as prospective materials for use in ultrashort-pulse laser systems.

Laser-Induced Damage in Optical Materials 2022, edited by Christopher Wren Carr, Detlev Ristau, Carmen S. Menoni, Proc. of SPIE Vol. 12300, 123000G
 · 0277-786X · doi: 10.1117/12.2641792

## 2. SAMPLE FABRICATION

### 2.1 Pulsed-laser deposition

The deposition of the films investigated in this study was performed with the PLD setup depicted schematically in Fig. 1 and described in more details in Refs. [15,26,31] The targets were fabricated by sintering powders of the materials of interest, which ensures a stoichiometric proportion of the elements, and had a final mass of $\sim 85\%$ of the expected mass for the pure crystalline material of the same volume. Target ablation was achieved using a KrF excimer laser operating at 248 nm, with a pulse duration of $\sim 30$ ns and a repetition rate of 100 Hz, yielding growth rates ranging from 10 µm/h ($Lu_2O_3$) to 20 µm/h ($Sc_2O_3$). The motion of the target was configured to obtain an effective bi-directional ablation, which was proven to significantly reduce the amount of scattering points in the as-grown films.[31]

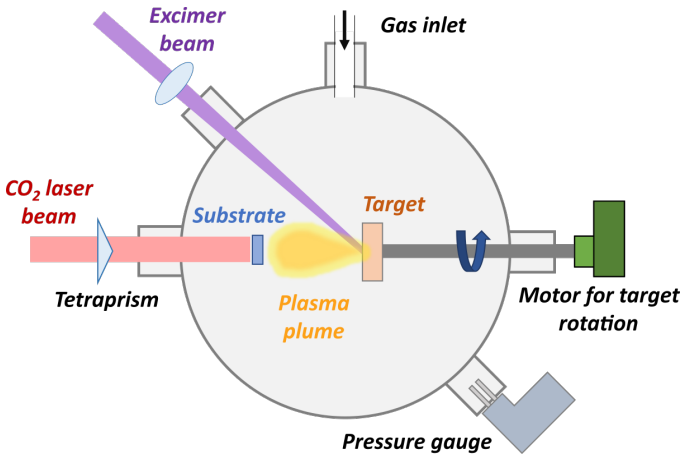


Figure 1. Pulsed-laser deposition setup.

To achieve crystalline-film growth, during deposition the rear surface of the substrate was heated by a $CO_2$ laser operating at 10.6 µm. The original Gaussian intensity distribution of the beam was transformed by a ZnSe tetraprism[32] into a nearly-uniform 10 x 10 mm square profile, which fits the substrate's dimensions. The substrate temperature used for the deposition of the samples ranged from 950°C to 1100°C, depending on the material.

The background pressure of the vacuum chamber could be tuned by manually adjusting an oxygen gas in-flow. All sesquioxide films analysed in this report were deposited at a background pressure of 20(±2) µbar.

The deposition parameters of the investigated samples are listed in Table 1. An optimisation of the parameters had been conducted previously and the samples for LIDT measurements were selected based on their crystalline properties and surface homogeneity (in terms of the number of scattering points visible under a dark field microscope).

Table 1. Deposition parameters and lattice properties of the sesquioxide films grown on sapphire ($Al_2O_3$) or yttrium aluminium garnet (YAG) substrates. The measurement of the XRD peaks and lattice constants are detailled in Sec. 3.2. The precision on the position of the (222) XRD peak is limited by the angular resolution of the incident beam, ±0.01°. The film lattice constant is calculated for a Cu K$\alpha$ wavelength of 1.5418 Å and the resolution error is ±0.004 Å.

| Substrate material & orientation | Film | Target ablation fluence | Heating power | (222) XRD peak position | Film lattice constant |
|---|---|---|---|---|---|
| YAG <100> | $Lu_2O_3$ | 1.21 J/cm$^2$ | 26.7 W | 29.79° | 10.390 Å |
| sapphire <0001> | $Lu_2O_3$ | 1.27 J/cm$^2$ | 26.2 W | 29.76° | 10.399 Å |
| sapphire <0001> | $Y_2O_3$ | 1.19 J/cm$^2$ | 18.0 W | 29.10° | 10.632 Å |
| sapphire <0001> | $Sc_2O_3$ | 1.24 J/cm$^2$ | 24.0 W | 31.50° | 9.840 Å |

### 2.2 Magnetron sputtering

Magnetron-sputtered samples were produced with a Helios coater developed by Bühler Leybold optics.[33] The layers were deposited by the plasma assisted reactive magnetron sputtering (PARMS) process. Inside the Helios coater, samples are placed on rotating plate. At first the sample passes under a mid frequency dual magnetron, where a thin substochiometric layer is deposited from a metallic target. Then the sample passes under radio frequency plasma source where the thin layer is oxidized. The PARMS process therefore produces high-density oxide coatings.[34] The speed of rotation and power of magnetron is adjusted to deposit $\sim 0.1$ nm of thin-film in each rotation. Each individual thin-film-layer thickness is controlled by in situ optical monitoring. Optical measurement is performed at each passing of the substrate under the measurement window. This allows the single-layer thickness to be controlled to better than 1 nm accuracy. Both monochromatic and broadband monitoring can be used in this setup.

Typical pressure inside the vacuum chamber during deposition is 50 nbar. An argon and oxygen mix is used as process gas for magnetron sputtering, while oxygen is used as the source gas in the plasma for thin-film oxidation. Both high and low index materials can be coated within one production cycle.

Previous studies have been conducted on films produced by this machine and their LIDT values compared to a large set of samples produced by different methods and manufacturers, exhibiting LIDT in accordance with state of the art.[1,24,35]

## 3. CHARACTERIZATION OF THE THIN FILMS

### 3.1 Samples to be tested

The tested samples were monolayers of $Y_2O_3$, $Sc_2O_3$, $Lu_2O_3$, $HfO_2$, $Nb_2O_5$ and $SiO_2$, see Table 2. The crystalline sesquioxide materials ($Y_2O_3$, $Sc_2O_3$, $Lu_2O_3$) were deposited on a <0001>-oriented sapphire substrate. In the case of $Lu_2O_3$ material, one sample was deposited on a <100>-oriented yttrium aluminium garnet (YAG) substrate. The amorphous metal oxides ($HfO_2$, $Nb_2O_5$, $SiO_2$) were deposited on fused silica (FS) using the magnetron sputtering process.

Table 2. Tested thin-film materials and their parameters, $n$ means refractive index at 1030 nm wavelength. The $Sc_2O_3$, $Y_2O_2$ and $Lu_2O_3$ sesquioxides were PLD-grown in the Optoelectronics Research Centre (Southampton, UK). The $HfO_2$, $Nb_2O_5$ and $SiO_2$ were magnetron-sputtered (MS) in the Institut Fresnel (Marseille, France). $^\star HfO_2$ is not pure but contains $\sim 1-2\,\%$ of $SiO_2$ admixture.[36] $^\dagger$The $SiO_2$ bandgap was taken from.[35]

| Material | Thickness | $n$ | Bandgap | Deposition | Substrate |
|---|---|---|---|---|---|
| $Sc_2O_3$ | 1750 nm | 1.97 | 5.74 eV | PLD | sapphire |
| $Y_2O_3$ | 1310 nm | 1.90 | 5.44 eV | PLD | sapphire |
| $Lu_2O_3$ | 970 nm | 1.91 | 5.43 eV | PLD | sapphire |
| $Lu_2O_3$ | 1000 nm | 1.91 | 5.43 eV | PLD | YAG |
| $HfO_2$ $^\star$ | 250 nm | 2.03 | 5.25 eV | MS | FS |
| $Nb_2O_5$ | 450 nm | 2.26 | 3.41 eV | MS | FS |
| $SiO_2$ | 450 nm | 1.47 | 8 eV $^\dagger$ | MS | FS |

#### 3.1.1 Refractive index measurement

The refractive indices of the magnetron-sputtered samples were determined by spectrophotometry using numerical fitting methods to the transmittance and reflectance measurements in the low-absorptance spectral region. The values of refractive indices at 1030 nm are listed in the Table 2. In the case of pulsed-laser deposited materials, the dispersion curves were determined using ellipsometry. The refractive indices of $Y_2O_3$ (1.90 @1030nm) and $Sc_2O_3$ (1.97 @1030nm) correspond well with published values.[37,38] Extinction coefficients were measured by ellipsometry, however given the uncertainty of the method, we can only assess that the extinction coefficient values are below $10^{-2}$ at 1030 nm.

### 3.1.2 Bandgap measurement

The optical bandgap values of the tested samples were derived from each film's intrinsic absorption coefficient, $\alpha$, by plotting $(\alpha E)^{1/2}$ as a function of the photon energy $E$ and extrapolating the linear curve to the abscissa axis. The bandgap error margins were estimated using the photon energies corresponding to absorption coefficients of $10^3$ and $10^4\,\mathrm{cm}^{-1}$.[39,40] The value of $SiO_2$ bandgap was taken from Ref. [35] because the absorption edge could not be reached with our instruments.

## 3.2 X-ray diffraction

Epitaxial growth of the $Y_2O_3$, $Lu_2O_3$ and $Sc_2O_3$ films on the <0001>-cut sapphire was expected to be predominantely in the <111>-direction, since the lattice mismatch in this orientation is the smallest with substrate orientation, i.e., 4.9 %, 2.9 % and 2.5 %, respectively. Similarly, $Lu_2O_3$ <111> has a quasi-perfect lattice match with <100>-cut YAG, that facilitates growth of that orientation.

The out-of-plane X-ray diffraction (XRD) patterns from the samples were recorded by a Rigaku Smartlab, equipped with a Ge(220) 2-bounce monochromator. Two different sets of parameters were selected for the scans. A wide scan with a 2Θ value from 20° to 80° and a step size of 0.02° was used to compare the proportion of the different orientations in the film. Since the films were expected to grow preferentially in the <111>-direction, the (222) diffraction peak was our main peak of interest. Secondly, an additional high-resolution scan with a step size of 0.002° was made around this primary peak.

Fig. 2 displays the XRD patterns of the films with each peak labelled with the corresponding orientation. The $Y_2O_3$ and $Sc_2O_3$ films grew primarily in the <111>-orientation, as demonstrated by the dominance of the (222) peak. The height ratio between the (222)-peak and the peaks corresponding to other orientations is

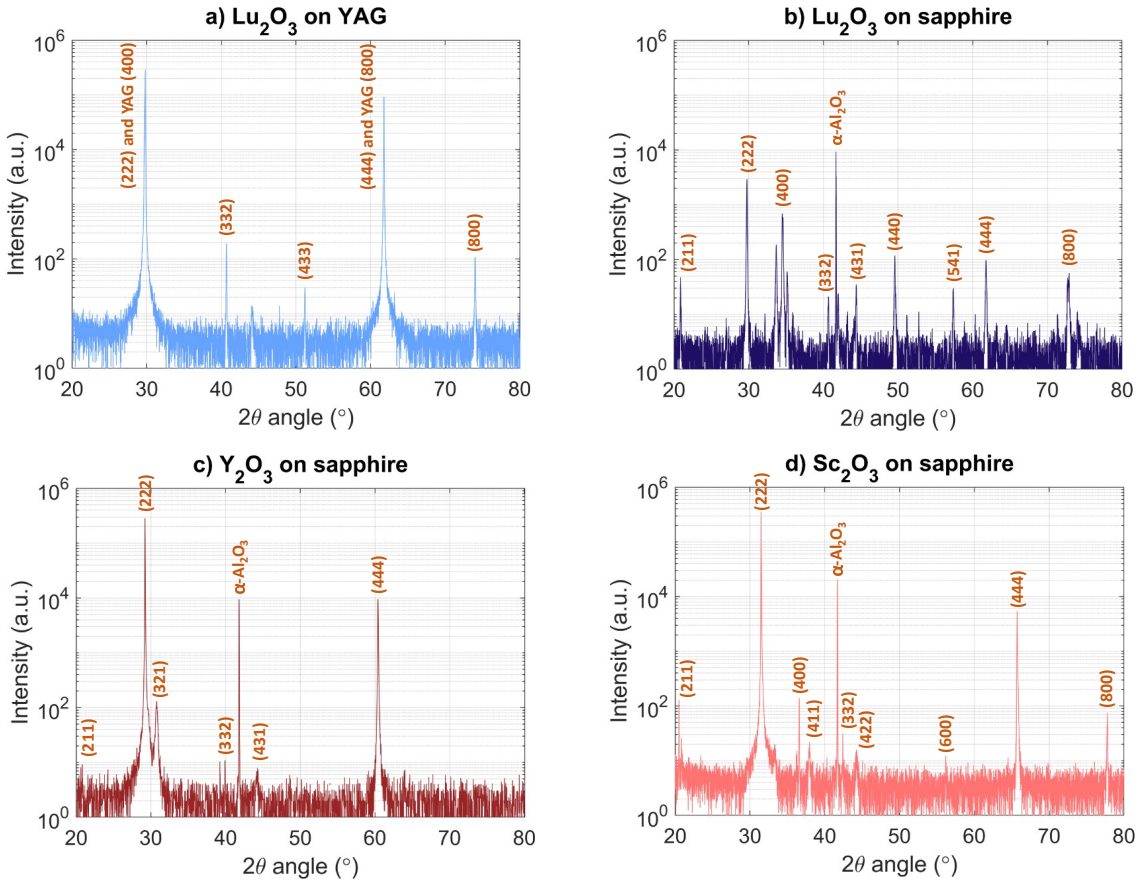


Figure 2. Wide XRD scans of the PLD samples: a) $Lu_2O_3$ film on YAG substrate, b) $Lu_2O_3$ film on sapphire substrate, c) $Y_2O_3$ film on sapphire substrate, d) $Sc_2O_3$ film on sapphire substrate.

greater than 3000. However, the $Lu_2O_3$ film grown on sapphire exhibits strong polycrystalline characteristics, with several orientations that have a height ratio of less than 30 with the (222) peak. On the contrary, the growth of <111>-oriented $Lu_2O_3$ is clearly favoured on the YAG substrate: the XRD figure shows also that the (222) peak is 1500-times stronger than the next visible orientation (332) and is nearly perfectly superimposed with the YAG (400) peak at a 2Θ angle of 29.8°. This aspect is highlighted in the high resolution XRD pattern of that sample in Fig. 3b), with a clear double-peak lying at 29.8°.

Fig. 3 compares the position of the (222) peak of the different films, which was used to calculate their lattice constants. The results, summarized in Table 1, show that the lattice constant of the as-grown films is close to the value reported for the corresponding bulk materials.[41,42]

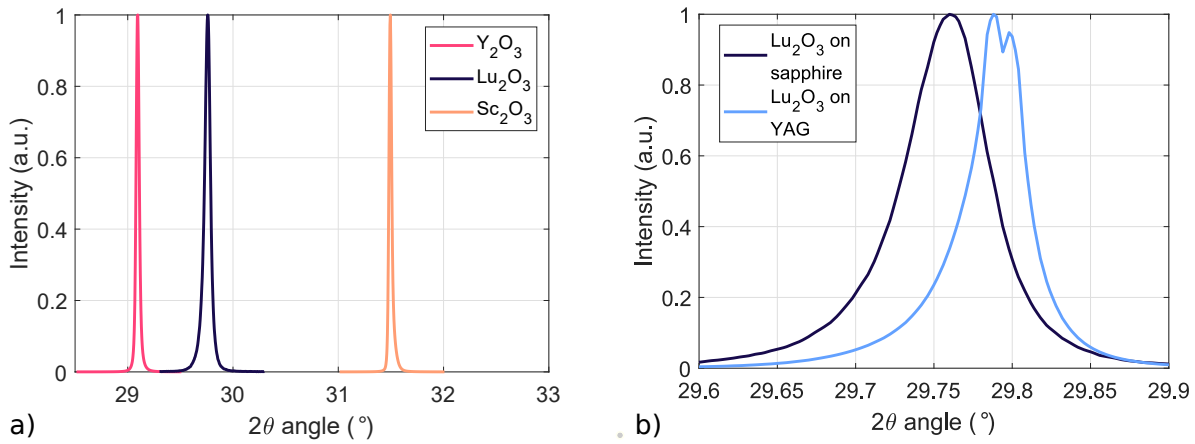


Figure 3. a) (222) XRD peaks of the $Y_2O_3$, $Lu_2O_3$ and $Sc_2O_3$ films grown on <0001>-sapphire; b) (222) XRD peak of the $Lu_2O_3$ films grown on <0001>-sapphire and <100>-YAG.

## 4. DESCRIPTION OF LIDT STATION AND TEST PROCEDURE

### 4.1 Test station

The test station used for LIDT tests is described in Ref. [43] detailing the description of test procedures and metrology methods. For the results reported here in this study, the pulses of nearly Gaussian spatial profile and ∼ 500 fs pulse duration at ∼ 1030 nm wavelength were incident at a repetition rate of 10 Hz. The maximum achievable pulse energy on a sample was 0.85 mJ. Characterization of the spatial and temporal profiles as well as an energy calibration were carried out before and after the LIDT test campaign. The LIDT tests were performed with samples placed at focal plane of the lens with 30-cm focal length. The effective beam diameter, as defined by international standards,[44] was 84 µm in a plane perpendicular to the beam propagation. The LIDT tests were performed in an air environment at a room temperature of 25 °C and humidity around 27 %. A typical spatial beam profile at the focal plane, autocorrelation trace and spectral distribution are shown in Fig. 4.

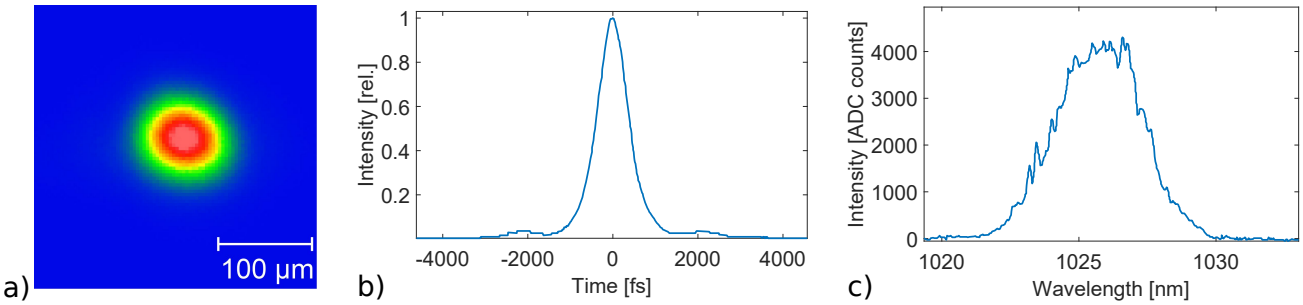


Figure 4. Laser beam characterization: a) beam profile in the focal plane, b) autocorrelation trace, c) spectral profile of laser at 1 kHz repetition rate. Effective beam diameter is 84 µm. Pulse duration FWHM is 525 fs (sech$^2$).

### 4.2 LIDT procedure and damage detection

Each sample was irradiated at different spots with unique pulse energies that were changed with a $\sim 1\,\%$ energy increment in order to get statistical data. The procedure was repeated for different numbers of pulses - from single-shot up to 1000 shots at 10 Hz. The LIDT tests were done at 45° incidence angle with P-polarization. The irradiated sites were analyzed ex-situ using a Zeiss Axiotech differential interference contrast microscope with 20x-objective magnification. Any observable material modification was evaluated as damage. The damage threshold was determined as the highest fluence that is lower than the lowest fluence causing damage in the experiment. The error bars correspond to sum of three standard deviations ($3\sigma$) of effective beam area near focal plane ($\sim 3\,\%$), pulse energy ($\sim 0.7\,\%$) and a half of pulse energy increment ($\sim 0.5\,\%$).

### 4.3 Intrinsic LIDT fluence

Since the optical layers are the scene of interference effects, the distribution of the electric field inside the layer irradiated by the laser is not homogeneous. The electric field distribution is critical for understanding sub-ps LIDT results, since the excitation of dielectrics is governed by electronic processes.[45] To compare LIDT results, accounting for the conditions influencing the electric field distribution, e.g., angle of incidence, polarization, layer thickness or refractive index, it is necessary to rescale the LIDT results with the electric field intensity maximum ($EFI_{\max}$) within the given layer. Therefore, the fluence values reported in this study correspond to $F_{\text{int}}$ intrinsic fluence determined using $F_{\text{ext}}$ external fluence and the $EFI_{\max}$:

$$F_{\text{int}} = EFI_{\max} \cdot F_{\text{ext}} = \left| \frac{E_{\max}}{E_{\text{inc}}} \right|^2 \cdot F_{\text{ext}}, \tag{1}$$

where the $E_{\max}$ represents the maximum value of electric field in the layer and the $E_{\text{inc}}$ means incident electric field amplitude.[46] The correction factor of incidence angle during the damage tests (45°) is taken into account within the $EFI_{\max}$ calculation. The distribution of the relative electric field intensity for the $Sc_2O_3$ layer used in our experiment is shown in Fig. 5.

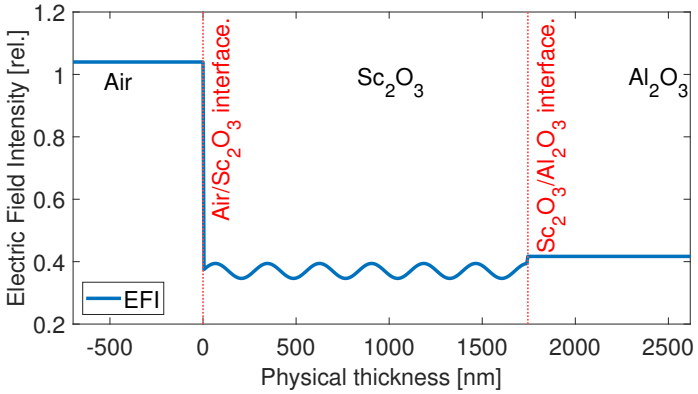


Figure 5. Distribution of the relative electric field intensity (EFI) inside a $Sc_2O_3$ layer of 1745 nm thickness (refractive index 1.97 at 1030 nm wavelength) deposited on a sapphire substrate (refractive index 1.78 at 1030 nm wavelength). Incident beam was P-polarized at an angle of incidence of 45°. The EFI is normalized to the incident electric field amplitude in air.

## 5. LASER DAMAGE RESULTS AND DISCUSSION

### 5.1 Deterministic 0-1 transition

To evaluate the uniformity of the tested materials in terms of laser damage, the transition range of the damage probability, as indicated in Fig. 6a), was calculated for each material and number of shots used, see Fig. 6b). The 1-on-1 laser damage tests with $Sc_2O_3$, $Y_2O_3$, $SiO_2$, $HfO_2$, $Nb_2O_5$ show deterministic results, i.e., narrow transition ranges of damage probability from 0 to 1. The transition range of damage probability was only a few percent in fluence, which suggests that the LIDT is limited by intrinsic material properties rather than by defects

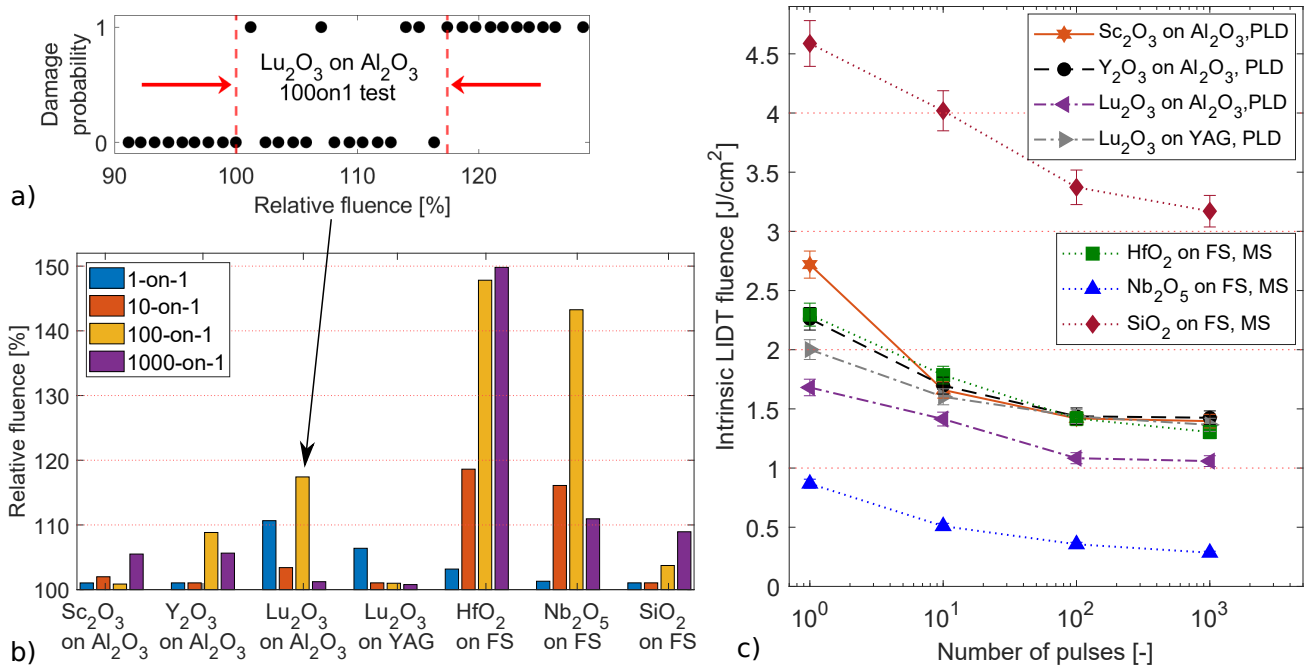


Figure 6. Laser damage results for materials used in GWS: a) example of the damage probability results in the case of 100-on-1 tests with $Lu_2O_3$ deposited on sapphire; b) transition ranges for the damage probability expressed in relative fluence, as indicated in Fig. 6a); c) intrinsic LIDT fluence as a function of shot number. The $Sc_2O_3$, $Lu_2O_3$, and $Y_2O_3$ films were fabricated by pulsed-laser deposition, while $HfO_2$, $Nb_2O_5$ and $SiO_2$ by magnetron sputtering. All samples were tested with pulse duration of 500 fs at 1030 nm.

or impurities caused by the deposition process.[47] However, in the case of $Lu_2O_3$ we found wider transition ranges that could be a consequence of film imperfections, especially in the case of the film grown on sapphire that could be connected to the polycrystalline nature of this film. The larger ranges for the multiple-pulse tests may be due to the stochastic formation of deep and shallow traps in the bandgap, which facilitate electron excitation and material modification.[45]

### 5.2 LIDT - single shots

The intrinsic LIDT fluence as a function of shot number for different thin-film materials is shown in Fig. 6c). Among the tested materials, the $SiO_2$ film shows the highest LIDT while $Nb_2O_5$ shows the lowest. In between, we find the other high-index materials, namely $HfO_2$, $Sc_2O_3$, $Y_2O_3$ and $Lu_2O_3$, that are interesting for high-power applications.

$HfO_2$, a widely used high-index material in optical mirrors, showed a single-shot LIDT of 2.3 J/cm$^2$, which is higher than the values around 2.0 J/cm$^2$ published in previous works[9,48,49] performed for conditions close to ones used in this study (1030 nm, 500 fs). The higher LIDT of the tested $HfO_2$ can be explained by the inclusion of $SiO_2$ in the deposited film, which was estimated from dispersion curve to be around 1-2 %.[36] The effect of the $SiO_2$ admixture on the $HfO_2$ damage threshold is in agreement with previous work.[1]

### 5.3 LIDT - multiple shots

For all materials, the LIDT is decreasing with an increasing number of shots, see Fig. 6c). The results show a drop of $> 20\%$ of the threshold within the first 100 shots. In contrast, at the transition from 100 pulses to 1000 pulses we observe only a small decrease. These tendencies were already observed in works performed at similar irradiation conditions with metal oxide coatings.[9,35,50] The gradual decrease is associated with the formation of laser-induced defects, leading to accessible energy levels within the bandgap. The deep or shallow traps can capture electrons from the conduction band even after a sub-threshold irradiation.[51]

In the case of $Sc_2O_3$, the drop in LIDT is more noticeable than for the other sesquioxides and reaches that of $HfO_2$. The larger 1-on-1 LIDT of $Sc_2O_3$ compared to $HfO_2$ was also observed in work with IBS films[19] which could be related to imperfect damage detection. Going to a higher number of pulses, the $HfO_2$ deposited on FS, $Y_2O_3$ on $Al_2O_3$, $Sc_2O_3$ on $Al_2O_3$, and $Lu_2O_3$ on YAG, samples show very similar LIDT, indicating that any of these materials could be recommended for high-power applications, as far as LIDT is concerned. The 1-on-1 and 100-on-1 LIDT values of $Y_2O_3$, $Sc_2O_3$ and $HfO_2$ materials were determined to be close to each other in the study,[9] devoted to electron-beam deposited single-layers on FS substrates. The LIDT tests were performed at identical conditions to this work (500 fs, 1030 nm, 10 Hz).

In the case of $Lu_2O_3$ deposited on an $Al_2O_3$ substrate, we observe significantly lower LIDT values, which could be explained by the polycrystalline and highly textured nature of the film. The presence of multiple crystal orientations implies the existence of discontinuities in the lattice that may potentially modify the local bandgap of the material. These boundaries between domains of different orientations may initiate the damage.

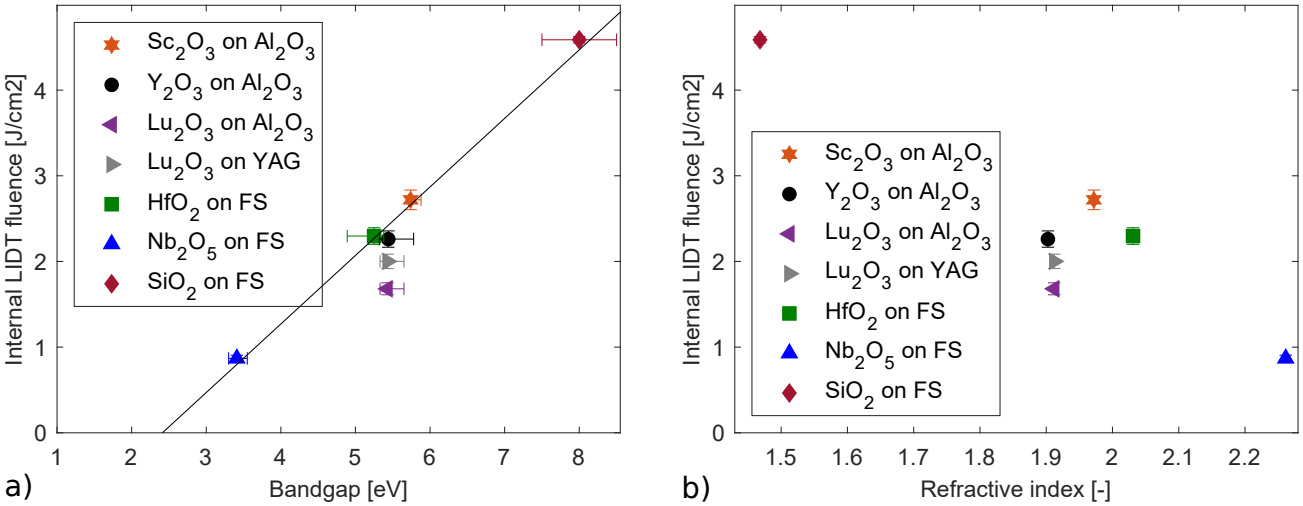


Figure 7. Single-shot intrinsic LIDT fluence as a function of material bandgap (a) and refractive index (b). The bandgap was determined using the Tauc method.

## 5.4 Bandgap

Since the laser-damage initiation in the sub-ps regime is driven by nonlinear ionization, the bandgap represents a critical parameter that correlates with the laser-damage resistance.[47] The behavior can be explained by taking into account the electron excitation processes playing a dominant role at the beginning of damage formation, i.e. multi-photon and impact ionization.[45] The intrinsic threshold fluences of tested materials are plotted as a function of their bandgap values in Fig. 7a). We observe a linear tendency of increasing single-shot LIDT with a larger bandgap value that is in agreement with the studies performed at similar irradiation conditions in Refs.[24, 52]

The deviations from the linear tendency in Fig. 7a) can be explained by the challenges faced to observe material modifications induced by single-shot irradiation. Moreover, some of the sesquioxide crystal films exhibit imperfections that include defect sites. For example, the lower LIDT of $Lu_2O_3$ on sapphire could have been caused by its polycrystalline structure, enabling lower local bandgap values at domain boundaries for different lattice orientations. It should be highlighted that the Tauc method provides a measure of the bandgap at a macroscopic scale, while on the microscopy level there are likely to be numerous defects in the polycrystalline film. Even in the case of the near single-crystal $Lu_2O_3$ on YAG, the error bars on the bandgap would be larger than that determined from the Tauc measurement method used.

In this work, the LIDT (in J/cm$^2$) tendency on bandgap $E_g$ (in eV) can be well fitted by the relation:

$$LIDT = 0.8 \times E_g - 1.93. \quad (2)$$

The equation shows a higher slope, i.e., more dynamic dependence on the bandgap than the empirical description in Ref.[24] derived from results for numerous materials deposited by various methods. The differences from the published data could be explained by the limited number of tested samples or the selected method of bandgap determination.

The bandgap values of sesquioxides are very close to each other with slightly larger bandgap in the case of $Sc_2O_3$, see Fig. 7, whose single-shot LIDT was determined as the highest within the high-index materials. The determined bandgap value for the $Sc_2O_3$ film tested (5.7 eV) is close to the bandgap of ion-beam sputtered $Sc_2O_3$ (5.6 eV).[19] However, larger bandgaps have been reported for electron-beam deposition (EBD) of $Sc_2O_3$ (6.5 eV) or $Y_2O_3$ (6.1 eV)[9] compared with the samples tested here grown by PLD i.e., $Sc_2O_3$ (5.7 eV) or $Y_2O_3$ (5.4 eV). It should be noted that care should be taken when comparing bandgaps across publications, since the bandgap is not exactly defined and can be determined using different methods.

### 5.5 Refractive index

For the design of multilayer components and GWS in our case, the critical parameter is the refractive index. Thus, in Fig. 7b), we plot the intrinsic 1-on-1 LIDT of the tested materials as a function of refractive index. The results confirm the trend of increasing refractive index with decreasing intrinsic 1-on-1 LIDT, which was also observed in works[1,24] performed at similar irradiation conditions (500 fs, 1030 nm). Amorphous and single-crystal materials appear to follow the trend, while polycrystalline sesquioxide, such as $Lu_2O_3$ on $Al_2O_3$, seems to be susceptible to a lower LIDT. This could be due to local defects associated with domain boundary interfaces and the highly textured surface. Based on the comparison, $Sc_2O_3$ seems to be the most promising of the sesquioxides, showing both high damage resistance and a high refractive index value. Furthermore, the pulsed-laser deposited $Sc_2O_3$ (1.97) shows higher refractive index at 1030 nm than the ion-beam sputtered one (1.93)[19] or the electron-beam deposited $Sc_2O_3$ (1.82).[9] The refractive index of the PLD $Y_2O_3$ samples studied here is same as that of EBD $Y_2O_3$ (1.90).[9]

## 6. CONCLUSION

$Sc_2O_3$, $Y_2O_3$ and $Lu_2O_3$ sesquioxide crystalline films, deposited by pulsed-laser deposition, were tested for sub-ps laser damage. Similar intrinsic LIDT fluences of 1.3 - 1.4 J/cm$^2$ were found for the well-grown sesquioxides, i.e. $Sc_2O_3$ on sapphire, $Y_2O_3$ on sapphire and $Lu_2O_3$ on YAG, when tested with multiple pulses (100 or 1k).

The LIDT tests on $Lu_2O_3$ grown on sapphire revealed significantly lower damage thresholds than $Lu_2O_3$ on YAG. This result is explained by the polycrystalline structure of $Lu_2O_3$ grown on sapphire, deduced from XRD characterization. The highly textured polycrystalline structure contains discontinuities in the lattice that most probably initiate the damage.

The high-index PLD sesquioxides show high bandgap values indicating good damage resistance in optical-coatings. In terms of observed damage thresholds, sesquioxides can compete with $HfO_2$, a frequently used high-index material in dielectric multilayers. The study shows that pulsed-laser deposition is a candidate for optical-coating fabrication and that the sesquioxides are promising high-index materials that could be used in applications relating to high-power ultrashort-pulse lasers.

### Acknowledgements

This project has received funding from the European Union's Horizon 2020 research and innovation programme under the Marie Skłodowska-Curie grant agreement No 813159. The authors acknowledge the EPSRC for financial support of the Rigaku SmartLab via grants (EP/K009877/1), (EP/K00509X/1) and (EP/V035975/1), an EPSRC Doctoral Prize EP/T517859/1, and grant nos. EP/N018281/1 and EP/P027644/1.

## REFERENCES

[1] Mangote, B., Gallais, L., Commandré, M., Mende, M., Jensen, L., Ehlers, H., Jupé, M., Ristau, D., Melninkaitis, A., Mirauskas, J., Sirutkaitis, V., Kičas, S., Tolenis, T., and Drazdys, R., "Femtosecond laser damage resistance of oxide and mixture oxide optical coatings," *Opt. Lett.* **37**, 1478 (May 2012). [doi:10.1364/OL.37.001478].

[2] Csajbók, V., Szikszai, L., Nagy, B. J., and Dombi, P., "Femtosecond damage resistance of femtosecond multilayer and hybrid mirrors," *Opt. Lett.* **41**, 3527 (Aug 2016). [doi:10.1364/OL.41.003527].

[3] Vanda, J., Ševčík, J., Pupka, E., Ščiuka, M., Melninkaitis, A., Divoký, M., Jambunathan, V., Bonora, S., Škoda, V., Lucianetti, A., Rostohar, D., Mocek, T., and Sirutkaitis, V., "Comparative LIDT measurements of optical components for high-energy HiLASE lasers," *High Power Laser Sci. Eng.* **4**, e11 (2016). [doi:10.1017/hpl.2016.11].

[4] Chen, S., Zhao, Y., Yu, Z., Fang, Z., Li, D., He, H., and Shao, J., "Femtosecond laser-induced damage of $HfO_2/SiO_2$ mirror with different stack structure," *Appl. Opt.* **51**, 6188 (Sep 2012). [doi:10.1364/AO.51.006188].

[5] Willemsen, T., Jupé, M., Gyamfi, M., Schlichting, S., and Ristau, D., "Enhancement of the damage resistance of ultra-fast optics by novel design approaches," *Opt. Express* **25**, 31948 (Dec 2017). [doi:10.1364/OE.25.031948].

[6] Chorel, M., Lanternier, T., Lavastre, E., Bonod, N., Bousquet, B., and Néauport, J., "Robust optimization of the laser induced damage threshold of dielectric mirrors for high power lasers," *Opt. Express* **26**, 11764 (Apr 2018). [doi:10.1364/OE.26.011764].

[7] Oliver, J. B., Bromage, J., Smith, C., Sadowski, D., Dorrer, C., and Rigatti, A. L., "Plasma-ion-assisted coatings for 15 femtosecond laser systems," *Appl. Opt.* **53**, A221 (Feb 2014). [doi:10.1364/AO.53.00A221].

[8] Willemsen, T., Jupé, M., Gallais, L., Tetzlaff, D., and Ristau, D., "Tunable optical properties of amorphous Tantala layers in a quantizing structure," *Opt. Lett.* **42**, 4502 (Nov 2017). [doi:10.1364/OL.42.004502].

[9] Hervy, A., Gallais, L., Chériaux, G., and Mouricaud, D., "Femtosecond laser-induced damage threshold of electron beam deposited dielectrics for 1-m class optics," *Opt. Eng.* **56**, 011001 (Jun 2016). [doi:10.1117/1.OE.56.1.011001].

[10] Craciun, F., Lippert, T., and Dinescu, M., "Pulsed Laser Deposition: Fundamentals, Applications, and Perspectives," in [*Handbook of Laser Micro- and Nano-Engineering*], Sugioka, K., ed., 1–33, Springer, Cham (2020). [doi:10.1007/978-3-319-69537-2_27-1].

[11] Masood, K. B., Kumar, P., Malik, M. A., and Singh, J., "A comprehensive tutorial on the pulsed laser deposition technique and developments in the fabrication of low dimensional systems and nanostructures," *Emergent Mater.* **4**, 737–754 (Jun 2021). [doi:10.1007/s42247-020-00155-5].

[12] Filipescu, M., Palla-Papavlu, A., Bercea, A., Rusen, L., Cernaianu, M. O., Ion, V., Calugar, A., Nistor, L. C., and Dinescu, M., "Antireflective coatings with high damage threshold prepared by laser ablation," *Appl. Phys. A* **125**, 815 (Dec 2019). [doi:10.1007/s00339-019-3110-y].

[13] Bercea, A., Filipescu, M., Moldovan, A., Brajnicov, S., Colgeag, D., Ion, V., Nistor, L. C., Zorilla, A., and Dinescu, M., "Optical coatings for ELI experiments prepared by laser ablation," *Rom. J. Phys.* **63**(606) (2018).

[14] Sirjita, E. N., Rusen, L., Brajnicov, S., Craciun, C., Ion, V., Filipescu, M., and Dinescu, M., "Properties of Hafnium and Aluminium Silicates Coatings Obtained by PLD," *Coatings* **11**, 753 (Jun 2021). [doi:10.3390/coatings11070753].

[15] Prentice, J. J., Grant-Jacob, J. A., Shepherd, D. P., Eason, R. W., and Mackenzie, J. I., "Yb-doped mixed-sesquioxide films grown by pulsed laser deposition," *J. Cryst. Growth* **491**, 51–56 (Jun 2018). [doi:10.1016/j.jcrysgro.2018.03.039].

[16] Sloyan, K. A., May-Smith, T. C., Zervas, M. N., and Eason, R. W., "Crystalline garnet Bragg reflectors for high power, high temperature, and integrated applications fabricated by multi-beam pulsed laser deposition," *Appl. Phys. Lett.* **101**, 081117 (Aug 2012). [doi:10.1063/1.4748107].

[17] Jensen, L. O., Mende, M., Blaschke, H., Ristau, D., Nguyen, D., Emmert, L., and Rudolph, W., "Investigations on $SiO_2/HfO_2$ mixtures for nanosecond and femtosecond pulses," in [*Proc. SPIE*], **7842**, 68 – 77 (Oct 2010). [doi:10.1117/12.867238].

[18] Lamaignère, L., Ollé, A., Chorel, M., Roquin, N., Kozlov, A. A., Hoffman, B. N., Oliver, J. B., Demos, S. G., Gallais, L., Negres, R. A., and Melninkaitis, A., "Round-robin measurements of the laser-induced damage threshold with sub-picosecond pulses on optical single layers," *Opt. Eng.* **60**, 031005–1 (Nov 2020). [doi:10.1117/1.OE.60.3.031005].

[19] Mende, M., Schrameyer, S., Ehlers, H., Ristau, D., and Gallais, L., "Laser damage resistance of ion-beam sputtered $Sc_2O_3/SiO_2$ mixture optical coatings," *Appl. Opt.* **52**, 1368 (Mar 2013). [doi:10.1364/AO.52.001368].

[20] Menoni, C. S., Krous, E. M., Patel, D., Langston, P., Tollerud, J., Nguyen, D. N., Emmert, L. A., Markosyan, A., Route, R., Fejer, M., and Rudolph, W., "Advances in ion beam sputtered $Sc_2O_3$ for optical interference coatings," in [*Proc. SPIE*], **7842**, 784202 (Oct 2010). [doi:10.1117/12.855604].

[21] Krous, E. M., Patel, D., Langston, P., Menoni, C. S., Markosyan, A., Route, R. K., Fejer, M. M., Nguyen, D., Emmert, L. A., and Rudolph, W., "Scandium oxide thin films deposited by dual ion beam sputtering for high-power laser applications," in [*Optical Interference Coatings*], FA10, OSA, Tucson, AZ, USA (2010). [doi:10.1364/OIC.2010.FA10].

[22] Grosso, D. and Sermon, P., "Scandia optical coatings for application at 351 nm," *Thin Solid Films* **368**, 116–124 (Jun 2000). [doi:10.1016/S0040-6090(00)00924-X].

[23] Aarik, J., Mändar, H., Kirm, M., and Pung, L., "Optical characterization of $HfO_2$ thin films grown by atomic layer deposition," *Thin Solid Films* **466**, 41–47 (Nov 2004). [doi:10.1016/j.tsf.2004.01.110].

[24] Gallais, L. and Commandré, M., "Laser-induced damage thresholds of bulk and coating optical materials at 1030 nm, 500 fs," *Appl. Opt.* **53**, A186 (Feb 2014). [doi:10.1364/AO.53.00A186].

[25] Beecher, S. J., Grant-Jacob, J. A., Hua, P., Prentice, J. J., Eason, R. W., Shepherd, D. P., and Mackenzie, J. I., "Ytterbium-doped-garnet crystal waveguide lasers grown by pulsed laser deposition," *Optical Materials Express* **7**, 1628 (May 2017). [doi:10.1364/OME.7.001628].

[26] Govindassamy, G. A., Prentice, J. J., Lunney, J. G., Eason, R. W., and Mackenzie, J. I., "Effect of laser repetition rate on the growth of $Sc_2O_3$ via pulsed laser deposition," *Appl. Phys. A* **128**, 577 (Jul 2022). [doi:10.1007/s00339-022-05698-4].

[27] Quaranta, G., Basset, G., Martin, O. J. F., and Gallinet, B., "Recent Advances in Resonant Waveguide Gratings," *Laser Photonics Rev.* **12**, 1800017 (Sep 2018). [doi:10.1002/lpor.201800017].

[28] Rumpel, M., Moeller, M., Moormann, C., Graf, T., and Ahmed, M. A., "Broadband pulse compression gratings with measured 99.7% diffraction efficiency," *Opt. Lett.* **39**, 323 (Jan 2014). [doi:10.1364/OL.39.000323].

[29] Vogel, M. M., Rumpel, M., Weichelt, B., Voss, A., Haefner, M., Pruss, C., Osten, W., Ahmed, M. A., and Graf, T., "Single-layer resonant-waveguide grating for polarization and wavelength selection in Yb:YAG thin-disk lasers," *Opt. Express* **20**, 4024 (Feb 2012). [doi:10.1364/OE.20.004024].

[30] Ahmed, M. A., Rumpel, M., Voss, A., and Graf, T., "Applications of sub-wavelength grating mirrors in high-power lasers," *Adv. Opt. Technol.* **1**, 381–388 (Jan 2012). [doi:10.1515/aot-2012-0036].

[31] Prentice, J. J., Grant-Jacob, J. A., Kurilchik, S. V., Mackenzie, J. I., and Eason, R. W., "Particulate reduction in PLD-grown crystalline films via bi-directional target irradiation," *Appl. Phys. A* **125**, 152 (Feb 2019). [doi:10.1007/s00339-019-2456-5].

[32] May-Smith, T. C., Muir, A. C., Darby, M. S. B., and Eason, R. W., "Design and performance of a ZnSe tetra-prism for homogeneous substrate heating using a $CO_2$ laser for pulsed laser deposition experiments," *Appl. Opt.* **47**, 1767–1780 (Apr 2008). [doi:10.1364/AO.47.001767].

[33] Depla, D., Mahieu, S., and Greene, J., "Sputter Deposition Processes," in [*Handbook of Deposition Technologies for Films and Coatings*], Martin, P. M., ed., ch. 5, 253–296, William Andrew Publishing, Boston, third ed. (2010). [doi:10.1016/B978-0-8155-2031-3.00005-3].

[34] Scherer, M., "Magnetron sputter-deposition on atom layer scale," *Vak. Forsch. Prax.* **21**, 24–30 (Aug 2009). [doi:10.1002/vipr.200900391].

[35] Douti, D.-B., Gallais, L., and Commandré, M., "Laser-induced damage of optical thin films submitted to 343, 515, and 1030 nm multiple subpicosecond pulses," *Opt. Eng.* **53**, 122509 (Aug 2014). [doi:10.1117/1.OE.53.12.122509].

[36] Hagedorn, H., Lehnert, W., Pistner, J., Scherer, M., and A., Z., "Plasma assisted reactive magnetron sputtering of demanding interference filters," in [*SVC TechCon 2012*], O–24 (2012).

[37] Nigara, Y., "Measurement of the optical constants of yttrium oxide," *Jpn J Appl Phys* **7**, 404–408 (Apr 1968). [doi:10.1143/jjap.7.404].

[38] Belosludtsev, A., Juškevičius, K., Ceizaris, L., Samuilovas, R., Stanionytė, S., Jasulaitienė, V., and Kičas, S., "Correlation between stoichiometry and properties of scandium oxide films prepared by reactive magnetron sputtering," *Appl. Surf. Sci.* **427**, 312–318 (Jan 2018). [10.1016/j.apsusc.2017.08.068].

[39] Stenzel, O., Wilbrandt, S., Schürmann, M., Kaiser, N., Ehlers, H., Mende, M., Ristau, D., Bruns, S., Vergöhl, M., Stolze, M., Held, M., Niederwald, H., Koch, T., Riggers, W., Burdack, P., Mark, G., Schäfer, R., Mewes, S., Bischoff, M., Arntzen, M., Eisenkrämer, F., Lappschies, M., Jakobs, S., Koch, S., Baumgarten, B., and Tünnermann, A., "Mixed oxide coatings for optics," *Appl. Opt.* **50**, C69–C74 (Mar 2011). [doi:10.1364/AO.50.000C69].

[40] Freeman, E. C. and Paul, W., "Optical constants of rf sputtered hydrogenated amorphous Si," *Phys. Rev. B* **20**, 716–728 (Jul 1979). [doi:10.1103/PhysRevB.20.716].

[41] Krankel, C., "Rare-Earth-Doped Sesquioxides for Diode-Pumped High-Power Lasers in the 1-, 2-, and 3-µm Spectral Range," *IEEE J. Sel. Top. Quantum Electron.* **21**, 250–262 (Jan 2015). [doi:10.1109/JSTQE.2014.2346618].

[42] Kuzminykh, Y., Kahn, A., and Huber, G., "$Nd^{3+}$ doped $Sc_2O_3$ waveguiding film produced by pulsed laser deposition," *Opt. Mater.* **28**, 883–887 (May 2006). [doi:10.1016/j.optmat.2005.09.051].

[43] Stehlík, M., Wagner, F., Zideluns, J., Lemarchand, F., Lumeau, J., and Gallais, L., "Beam-size effects on the measurement of sub-picosecond intrinsic laser induced damage threshold of dielectric oxide coatings," *Appl. Opt.* **60**, 8569–8578 (Sep 2021). [doi:10.1364/AO.433935].

[44] ISO 21254-1:2011, "Lasers and laser-related equipment – test methods for laser-induced damage threshold – part 1: Definitions and general principles," tech. rep., International Organization for Standardization, Geneva, Switzerland (July 2011).

[45] Emmert, L. and Rudolph, W., "Femtosecond Laser-Induced Damage in Dielectric Materials," in [*Laser-Induced Damage in Optical Materials*], Ristau, D., ed., 127–152, CRC Press, Boca Raton, FL (Dec 2014). [doi:10.1201/b17722-7].

[46] Ohta, K. and Ishida, H., "Matrix formalism for calculation of electric field intensity of light in stratified multilayered films," *Appl. Opt.* **29**, 1952 (May 1990). [doi:10.1364/AO.29.001952].

[47] Mero, M., Liu, J., Rudolph, W., Ristau, D., and Starke, K., "Scaling laws of femtosecond laser pulse induced breakdown in oxide films," *Phys. Rev. B* **71**, 115109 (Mar 2005). [doi:10.1103/PhysRevB.71.115109].

[48] Hervy, A., Gallais, L., Mouricaud, D., and Chériaux, G., "Electron-beam deposited materials for high-reflective coatings: Femtosecond LIDT," in [*Optical Interference Coatings (OIC) 2013*], FA.4, OSA, Whistler, Canada (2013). [doi:10.1364/OIC.2013.FA.4].

[49] Gallais, L., Mangote, B., Zerrad, M., Commandré, M., Melninkaitis, A., Mirauskas, J., Jeskevic, M., and Sirutkaitis, V., "Laser-induced damage of hafnia coatings as a function of pulse duration in the femtosecond to nanosecond range," *Appl. Opt.* **50**, C178–C187 (Mar 2011). [doi:10.1364/AO.50.00C178].

[50] Nguyen, D. N., Emmert, L., Mero, M., Rudolph, W. G., Patel, D., Krous, E., and Menoni, C. S., "The effect of annealing on the subpicosecond breakdown behavior of hafnia films," in [*Proc. SPIE*], **7132**, 71320N (Oct 2008). [doi:10.1117/12.804452].

[51] Emmert, L. A., Mero, M., and Rudolph, W., "Modeling the effect of native and laser-induced states on the dielectric breakdown of wide band gap optical materials by multiple subpicosecond laser pulses," *J. Appl. Phys.* **108**, 043523 (Aug 2010). [doi:10.1063/1.3457791].

[52] Mangote, B., Gallais, L., Zerrad, M., Lemarchand, F., Gao, L. H., Commandré, M., and Lequime, M., "A high accuracy femto-/picosecond laser damage test facility dedicated to the study of optical thin films," *Phys. Rev. B* **83**, 013109 (Jan 2012). [doi:10.1063/1.3677324].